Power converter junction temperature measurement using infra-red sensors

Christopher J. Smith[1], Donatella Zappalá[1], Christopher J. Crabtree[1] ✉, Justo Lapiedra[2], Brian Mulholland[2]

[1]Durham University, UK
[2]Anecto, Ireland
✉ E-mail: c.j.crabtree@durham.ac.uk

Abstract: Studies demonstrate that the power converter has one of the highest failure rates in a wind turbine, with a key failure driver being the power module junction temperature (T_j). This paper details an experimental setup for simplified emulation of wind turbine conditions on a power converter with infra-red sensing of IGBT T_j. Results are compared to previous simulation work for a PMSG wind turbine, with the same trend of increasing mean T_j with wind speed found, and the need to use an equivalent generator reactance in highlighted. A commercial-scale prototype for more accurate wind turbine converter emulation is also detailed.

1 Introduction

Studies have shown that the power converter has one of the highest failure rates in a wind turbine [1]. Furthermore, the converter failure rate increases with turbine power rating and wind speed due to higher stressing and a higher number of components [2]: the current trend in offshore wind farms. Therefore, the converter, particularly in permanent-magnet synchronous generator turbines [3], is reliability-critical and must be understood in order to maximise the impact of improving reliability on the levelised cost of energy from wind.

Power module failure is the failure mode for nearly all major converter repairs [2]. Traditionally, power module failure has been linked to power module thermal loading, where the variation of temperature in the insulated gate bipolar transistors (IGBT) and diode cases causes fatigue through expansion and contraction between package layers [4]. The reference temperature is the virtual junction temperature (T_j), which is a virtual representation of the chip p-n junction temperature [4]. T_j variation is deemed the most important aspect to measure for physics-of-failure reliability analysis.

Present converter lifetime estimations and simulation models are validated using only static operating conditions with fixed currents and frequencies [5]. In reality, wind turbines have constantly varying frequency, voltage, and current throughputs due to the stochastic nature of the wind and the reactionary turbine controllers. There is, therefore, uncertainty over the applicability of present approaches for determining the suitability of converter designs to surviving electrical loading characteristics offshore.

In response, a holistic approach to wind turbine power converter reliability is proposed. This includes a combination of effective drive train modelling, simulation, and physical emulation of the power converter and its junction temperature (T_j) response under realistic wind turbine operating conditions. This will allow for developments in either computational or experimental fields to inform the formulation of results of the other.

Previous research by the authors has provided drive train modelling and thermal loading simulation [4]. This paper outlines the wind turbine power converter physical emulation and surrounding drive train to answer the following research questions (RQ):

(i) How should the device temperature be monitored to provide high-frequency, high-accuracy T_j measurements without affecting the control or operation of the device under test? (Section 2)

(ii) How can wind turbine operating conditions be emulated in a scaled down test bench? (Section 3, 4)

(iii) How do the results of simulation and physical testing compare? (Section 5)

(iv) How can this experimental rig be implemented for commercial scale device testing and certification? (Section 6)

2 Junction temperature measurement

To answer RQ1, this section reviews current methods for temperature measurement, determines the most suitable approach, and describes the realised thermal measurement experimental set up.

2.1 Measurement approach selection

There are three main approaches to temperature monitoring: direct contact, proxy using temperature-sensitive electrical parameters, or infra-red (IR) measurement.

Direct contact can be carried out using a thermocouple or thermistor. As thermocouples rely on conduction, they require direct adhesion to the device under test (DUT), and typically have slow response times of hundreds of ms [6] making them unsuitable for high-frequency temperature measurements as required by this research.

Temperature sensitive electrical parameters use measurable device voltages and currents to estimate the temperature of the power module. Some examples include the measurement of collector-emitter saturation voltage (V_{ces}), gate-emitter voltage (V_{ge}), and saturation current (I_{css}) [7]. In all cases, a small measurement signal is needed that is independent of normal operating conditions. Therefore, to be used in a functional environment, the converter control requires complex changes and the measured signals are susceptible to the noisy converter electromagnetic environment. This makes the approach impractical and it is not considered further.

IR measurement relies on capturing the IR radiation emitted by a body. The spectral content is determined by the temperature of the body and the emissivity of the body's surface. This relationship is well documented and can be calculated using Planck's law for a black body (emissivity (e) of 1). Therefore, by measuring the spectral radiance from a body over a specified wavelength range using a photoconductive sensor and correcting for output by the emissivity of the body (as a percentage of the radiance from a
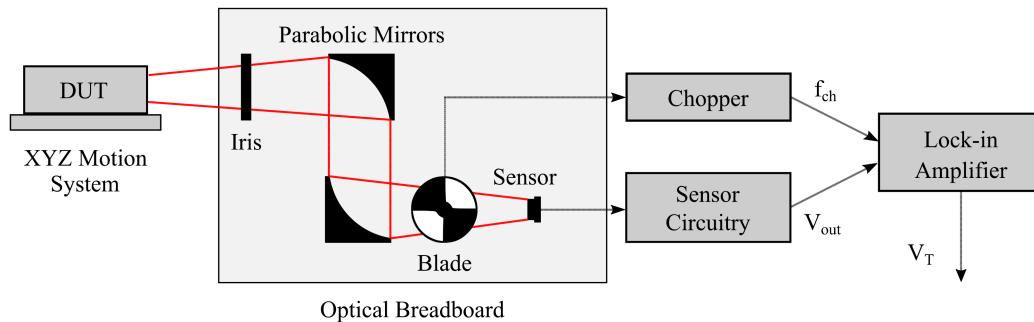
Fig. 1 *Experimental optical set-up. V_T is the temperature dependent voltage output and f_{ch} is the chopping frequency*
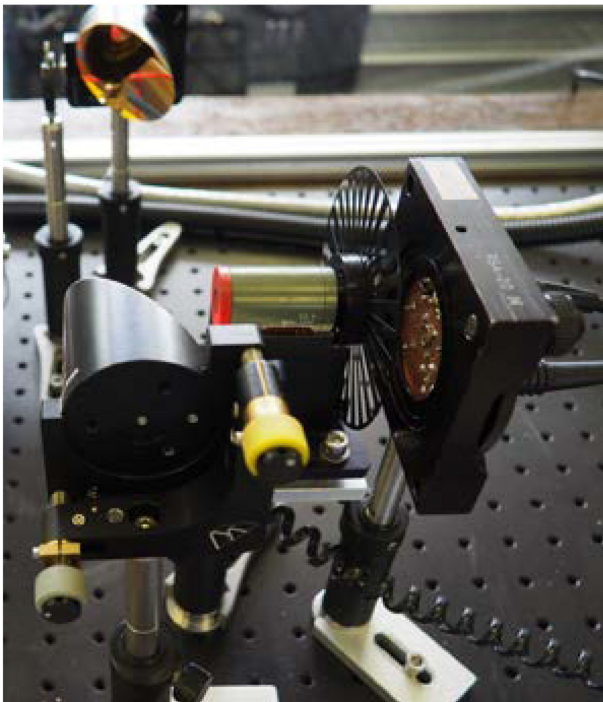

Fig. 2 *Photograph of optical set-up*

black body), the temperature can be measured without physical contact with the body.

IR measurement comes in two main forms; IR cameras and IR sensors. The outputs of an IR camera are recognisable by their multi-coloured images, providing an array of temperature measurements across a surface. Unfortunately, IR cameras are very expensive, particularly when fast response times and accurate temperature measurements are required, making them unsuitable for this experimental work. In contrast, IR sensors are essentially single pixel IR cameras and are subsequently less expensive. They are also able to measure spot temperatures more accurately, making them ideal for use in T_j monitoring in the power module.

IR approaches have some disadvantages. Although requiring no physical contact with the measured device, line of sight is required. This requires modification of the measured device through removal of its protective casing, as discussed in Section 3.2.

2.2 Experimental set-up

With an IR sensor approach chosen, the temperature measurement setup was developed to enhance the output of the IR sensor. The schematic of this setup is shown in Fig. 1. The key aspects of the optical set up are:

- *The IR sensor* is a Thor Labs PbSe photoconductive IR sensor [8] with a spectral measurement range of 1–4.8 µm and a response time of 10 µs.
- *The mirrors*. For rig flexibility, parabolic mirrors were used to focus the IR radiation from the DUT.

- *The XYZ position system* allows for precise positioning of the DUT to ensure repeatable testing and accuracy.
- *The chopper and lock-in amplifier*. As IR sensors are supplied with a high DC voltage (100 V), they have inherent DC bias on their output that can interfere with the measurement. To remove this bias, and to reduce background noise, an optical chopper is used to shift the temperature signal to 3.5 kHz. A lock-in amplifier is used as a band-pass filter linked to the chopper.

Fig. 2 presents a photograph of the optical set up.

The lock-in amplifier voltage output V_T in Fig. 1 is converted to a temperature measurement using a parabolic calibration curve derived from a range of temperature measurements taken by a FLIR C2 camera.

3 Drive train set-up

With the temperature measurement ready, wind turbine emulation was required. This included selecting an appropriately scaled DUT, preparing the DUT for measurement, scaling the DC link to emulate the larger wind turbine DC link, controlling the DUT, and mitigating noise issues. The schematic diagram of the experimental rig is provided in Fig. 3.

3.1 DUT selection

In [4], two parallel SEMIKRON SKSB2100GD69/11-MAPB stacks were used containing SKiiP2013GB172-4DWV3 half-bridge SKiiP modules. Ideally, these modules would be the DUT but this was impractical due to the cost and experimental impracticality of current and voltage ratings (1000 A_{nom} and 1700 V_{ces}).

A lower rated power module was required to operate within the available laboratory infrastructure. The power module selected was the SEMIKRON 01NAC066V3 MiniSKiiP module [9], which has lower current and voltage ratings (6 A_{nom} and 600 V_{ces}) and lower unit cost while still using the Trench3 IGBT technology found in the larger device, allowing for practical but realistic laboratory testing.

The key limitation of the 01NAC066V3 module is the packaging technology; the SKiiP2013 uses SKiNTER technology which replaces solder with cold-welded silver chip, and has the gate drivers incorporated into the package [10]. However, according to expert advice, this increases the lifetime of the device but does not change the fundamental failure modes, meaning that the 01NAC066V3 module was suitable for emulation of the large modules found in MW-scale turbines.

3.2 Device preparation

The device comes with a plastic case that uses sprung metallic legs to connect to the device and it is coated in an insulating silicon gel to avoid flash over. One of the main challenges with the chosen temperature measurement approach is the need to have line-of-sight to the IGBTs. To achieve this, the case was removed and the sprung metallic legs were replaced with direct solder joints. This direct soldering required the silicon gel to be removed by placing the whole device in a dodecylbenzenesulfonic acid bath for 24–48
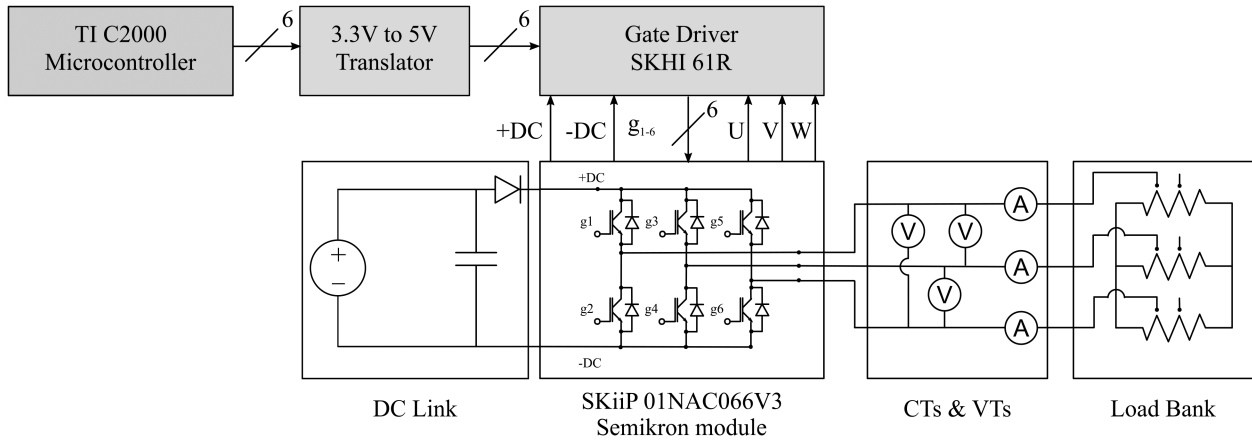
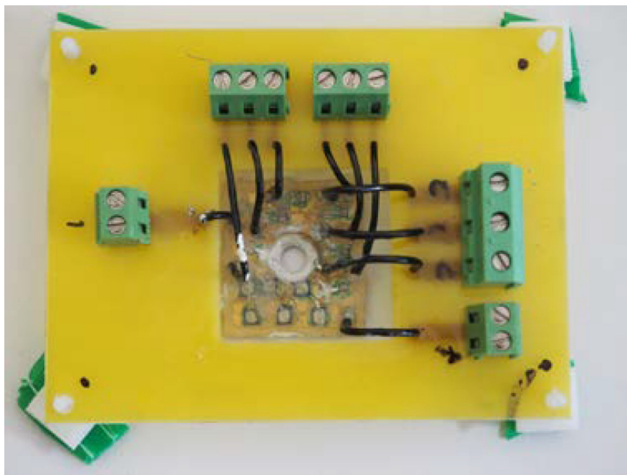**Fig. 3** *Electrical circuit diagram of the experimental rig*

Fig. 4 *SEMIKRON 01NAC066V3 MiniSKiiP module modified for testing*

Table 1 Power module voltage parameters

Parameter	Value
$V_{ces,e}$	600 V
$V_{ces,f}$	1700V
$V_{DC,e}$	406 V
$V_{DC,f}$	1150V

h. The connections were then soldered to the device, the silicon gel reapplied, and the device secured to a heat-sink with a nylon screw and thermal paste (Fig. 4).

3.3 DC link

As the DUT collector-emitter saturation voltage (V_{ces}) is lower than that of the MW-scale power modules, the DC link voltage must be scaled accordingly. Then, (1) can be applied to determine the equivalent DC-link voltage.

$$V_{DC,e} = V_{ces,e}(V_{ces,f})^{-1}V_{DC,f} \qquad (1)$$

where $V_{ces,e}$ and $V_{ces,f}$ are the experimental and full-scale power module collector-emitter saturation voltages, respectively, and $V_{DC,e}$ and $V_{DC,f}$ are the experimental and full-scale DC-link voltages, respectively. The values are given in Table 1.

A switch mode power supply with an output capacitor was used to emulate the DC link (Fig. 3). Due to equipment limitations, the DC-link voltage could only be set to a maximum of 300 V but this was deemed reasonable as it was assumed that the current throughput would have the greater impact on thermal loading.

3.4 Control circuitry

To invert the DC-link voltage, the six IGBTs were switched using sine wave pulse width modulation (SPWM) at 2 kHz. The SPWM was generated using a Texas Instruments micro-controller interfaced with MATLAB/Simulink to allow the use of in-built function blocks. The voltage was controlled in an open-loop configuration with the required voltage set in software and uploaded to the micro-controller.

3.5 Noise

Due to the high-frequency noise generated by switching, there were a number of issues with interference on both the gate driver and the temperature measurement output. To mitigate this, the following steps were taken:

- Isolated grounding and braiding for power circuitry, control circuitry, and measurement circuitry.
- Metallic shielding for control circuitry.
- Load bank placed away from the experiment.
- Power and gate driver cables kept perpendicular.

4 Wind turbine condition emulation

To replicate the fixed wind speeds in [4], the operating conditions have to be scaled to match the experimental constraints. The constant 12.7 m/s wind speed conditions simulated in [4] could not be replicated as the DC source did not have the current or voltage capacity required (5 A instead of 6 A, and 300 V instead of 406 V). The load bank's discrete resistances also meant that independent control of voltage and current was impossible, and the modulation index, m, would have to change to accommodate the different maximum voltages available. Current was given priority, and the voltage was varied as required as the losses are driven by the collector current.

The simulation parameters and their physical test equivalents are given in Table 2. m_f is the full-scale modulation index, m_e is the experimental modulation index, $I_{c,f}$ is the full-scale IGBT collector current, $I_{c,e}$ is the experimental IGBT collector current, and R_L is the load resistance. $I_{c,e}$ was calculated by using the ratio between rated $I_{c,e}$ and rated $I_{c,f}$ (6/2800) [6], and m_e was set so that the scaled equivalent AC voltage matched the full-scale AC voltage output.

5 Results and discussion

With the experimental rig constructed, the first stage was to verify the experimental rig outputs. Following this, to answer RQ3, the results from [4] are compared with the experimental results.

Table 2 Experimental test parameters and values for four wind speeds

Wind speed, m/s	Frequency, Hz	$V_{DC,f}$ (V)	$V_{DC,e}$ (V)	m_f	m_e	$I_{c,f}$ (A)	$I_{c,e}$ (A)	R_L, Ω
4	3.1	1150 V	300 V	0.28	0.57	323A	0.56	150
6	4.6	1150 V	300 V	0.42	0.67	483A	1.26	80
8	6.1	1150 V	300 V	0.55	0.79	633A	2.24	52
10	7.7	1150 V	300 V	0.72	0.93	828A	3.50	40
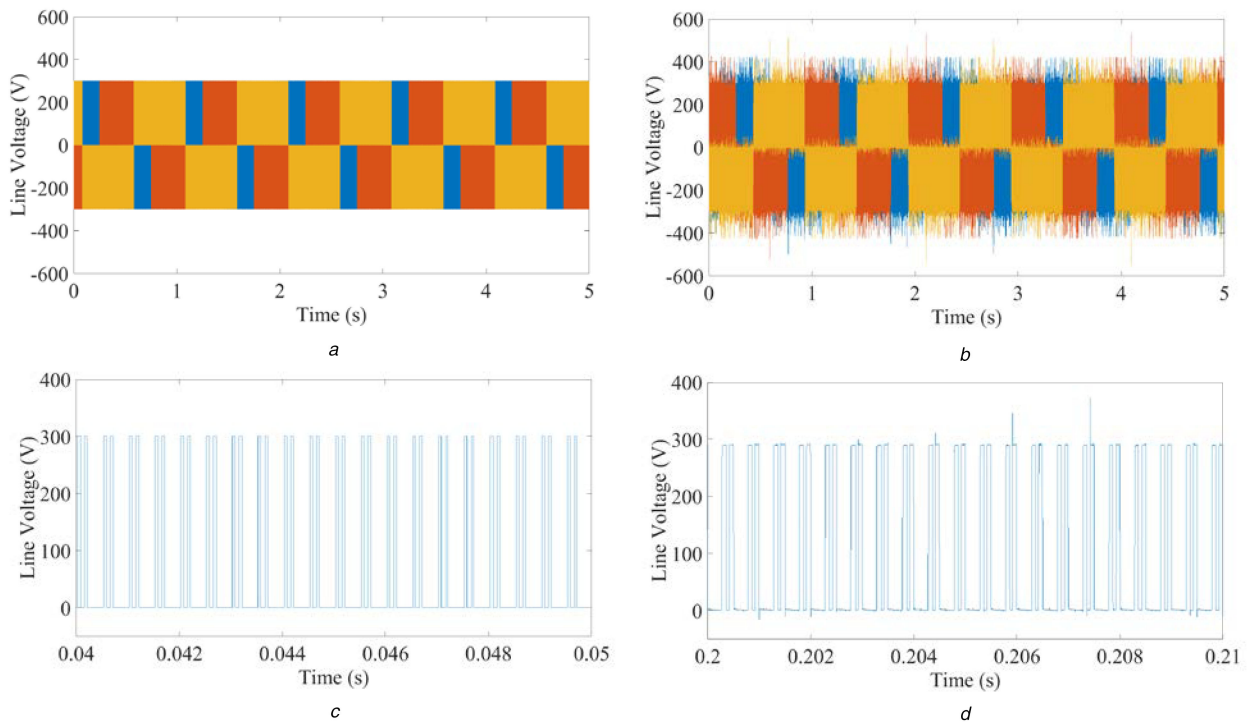
Fig. 5 *Verification of 3-phase voltage output*
(a) Simulated voltage, *(b)* Measured voltage, *(c)* Zoomed-in simulated voltage, *(d)* Zoomed-in experimental voltage
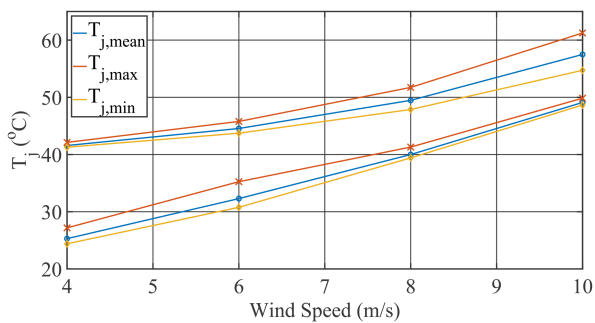
Fig. 6 T_j *results for equivalent wind speed tests. Dashed lines are simulated results and solid lines and experimental results*

5.1 Experimental verification

To verify that the experimental rig was producing expected voltage and current profiles, the experimental rig (Fig. 3) was modelled and simulated in Simulink. The same conditions were then applied to both model and rig and the voltage and current waveforms compared.

The simulated and experimental voltage waveforms were compared at 300 V with a 32 Ω star-connected resistive load with an output frequency of 1 Hz (Fig. 5). Unsurprisingly, the simulated three-phase voltage output is cleaner (Fig. 5a) than that of the experimental rig (Fig. 5b) as the simulation assumes that the IGBTs are perfect switches. In contrast, the real IGBTs are imperfect and produce short voltage transients when switching. However, both produce very similar magnitude waveforms and Figs. 5c and d reveal that individual voltage changes are consistent between simulation and experiment, validating the experimental rig output.

5.2 Comparison with simulation results

Experimental IGBT mean, maximum and minimum T_j resulting from the conditions in Table 2 are summarised in Fig. 6 alongside equivalent simulation results. The rise in mean temperature with wind speed confirms the increase found in [4]. This is because the overall device power losses increase with increased power throughput of the device.

However, unlike the simulation where the ΔT_j increased with increasing wind speed, in this case ΔT_j actually reduced. At first glance, this seemingly disproves the results in [4]. However, this result can be explained by the use of a resistive load in the experimental rig. The average I_c increased with increasing wind speed, increasing the total power losses experienced by the device and, therefore, raising the mean T_j. However, the instantaneous I_c when the device is switching is still 5 A regardless of the average I_c, causing the instantaneous switching power losses to remain relatively constant.

Therefore, as m increases with increasing wind speed, there are fewer switching events occurring per cycle, causing lower overall switching power losses. This in turn creates a lower ΔT_j with increasing wind speed.

In contrast, the inductive load in the simulations acts as a low-pass filter, smoothing the current throughput, reducing the instantaneous I_c experienced at switching events, particularly at lower wind speeds, and, therefore, reducing the switching losses at lower wind speed.

These results validate that the mean temperature will increase with increasing wind speed in a PMSG power module, and highlight the importance of providing an equivalent reactive load to emulate the power module conditions in future testing.
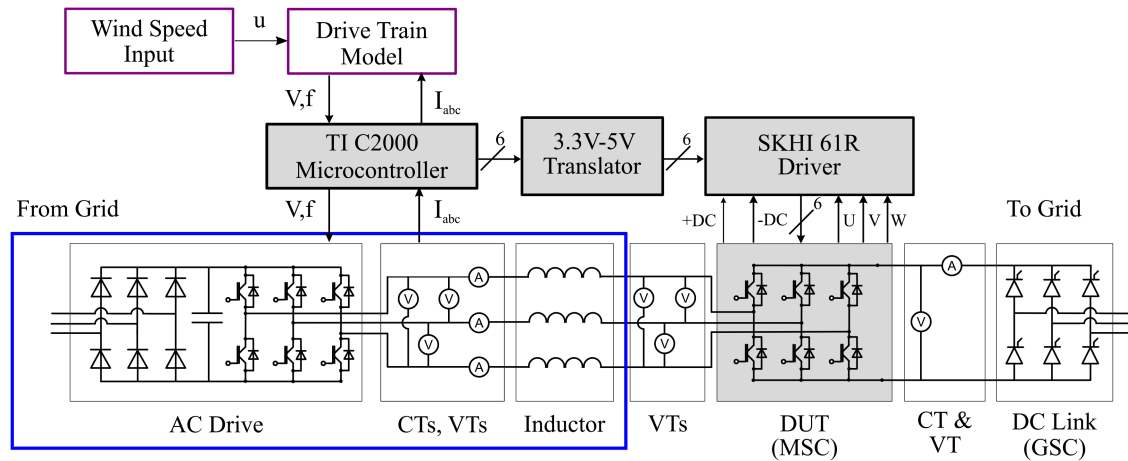
Fig. 7 *Test bench to allow variable wind condition testing*

6 Ongoing research: commercial test bench

This paper has provided a starting point for power converter reliability testing, but has highlighted a need for more advanced, larger scale testing of devices. In response, Anecto have supported an ongoing research project to construct a larger rig to emulate more realistic variable wind turbine operating conditions applied to a power converter in a laboratory environment.

This rig is based on the test bench described here, with several changes implemented to extend the operational range for more realistic, industrial-scale testing. Fig. 7 details the configuration of the larger wind turbine emulation rig. There are a number of enhancements over the current setup to the rig planned and under construction:

- The current has been reversed so that the DUT is configured as a rectifier as it is in simulation.
- To emulate a wind turbine drive train and generator (a requirement from Section 5.2), an AC–AC converter and inductor bank have been added that act as the generator armature and reactance, respectively.
- The load bank in Fig. 3 has been replaced with a DC link for regeneration.
- The control has been significantly expanded to allow for closed-loop control of the AC–AC converter and DUT to emulate wind turbine conditions more closely by allowing varying conditions. Much of this control is based on the model constructed in [4].

The test bench is designed to test a 600 V_{ces}, 30 A MiniSKiiP 15AC066V1 power module [11] to examine the impact of scaling factors on the temperature results as compared to the 6 A device. There is also scope to test at wind turbine drive train currents at ANECTO's industrial facilities once the intermediate rig has been constructed and validated.

7 Conclusions

A holistic approach to wind turbine power converter reliability is proposed. This includes a combination of effective drive train modelling, simulation, and physical emulation of the power converter and its junction temperature (T_j) response under realistic wind turbine operating conditions. This paper provides details of the experimental rig construction and validation.

Power module failure has been linked to power module thermal loading. As such, a unique approach of using high-frequency, low-cost PbSe photoconductive IR sensors has been used to capture the fundamental frequency temperature variations on a simplified drive train rig in the laboratory.

The results were compared to simulations in previous work. The increase in mean T_j of the IGBT in the simulations was validated experimentally, and the results highlighted the need to incorporate the reactive component of the PMSG. This led to a proposed commercial test bench being constructed in collaboration with Anecto to bring more realistic testing regimes to the wind industry.

8 Acknowledgments

9 References

[1] Spinato, F., Tavner, P.J., van Bussel, G.J.W.*, et al.*: 'Reliability of wind turbine subassemblies', *IET Renew. Power Gener.*, 2009, **3**, pp. 387–401

[2] Carroll, J., McDonald, A., McMillan, D.: 'Reliability comparison of wind turbines with DFIG and PMG drive trains', *IEEE Trans. Energy Convers.*, 2015, **30**, (2), pp. 663–670

[3] Xie, K., Jiang, Z., Li, W.: 'Effect of wind speed on wind turbine power converter reliability', *IEEE Trans. Energy Convers.*, 2012, **27**, pp. 96–104

[4] Smith, C.J., Crabtree, C.J., Matthews, P.C.: 'Impact of wind conditions on thermal loading of PMSG wind turbine power converters', *IET Power Electron.*, Accepted Manuscript, 2017, **10**, 11, pp. 1268–1278

[5] Wintrich, A., Nicolai, U., Tursky, W.*, et al.*: '*Application manual power semiconductors*' (SEMIKRON International GmBH, Nuremberg, Germany, 2015)

[6] RS: 'RS pro k type thermocouple glass fibre 2 m 0.3 mm diameter −50°C + 750°C', 2017. Available at http://uk.rs-online.com/web/p/products/6212170/

[7] Avenas, Y., Dupont, L.: 'Evaluation of IGBT thermo- sensitive electrical parameters under different dissipation conditions-comparison with infrared measurements', *Microelectron. Reliab.*, 2012, **52**, (11), pp. 2617–2626

[8] Thorlabs: 'Fdpse2 × 2 lead selenide photoconductor user guide', 2017. Available at https://www.thorlabs.com/drawings/c7b0c7db2ebcb5c-75C9AC04-5056-2306-D929B1EBB3AF0DB5/FDPSE2X2-Manual.pdf

[9] SEMIKRON: 'Skiip 01nac066v3', 2017. Available at https://www.semikron.com/dl/service-support/downloads/download/semikron-datasheet-skiip-01nac066v3-25232340/

[10] SEMIKRON: 'Skinter technology', 2015. Available at http://www.semikron.com/innovation-technology/construction-and-connectiontechnology/skinter-technology.html

[11] SEMIKRON: 'Skiip 15nac066v1', 2017. Available at https://www.semikron.com/dl/service-support/downloads/download/semikron-datasheet-skiip-15ac066v1-25230700/